THE JOURNAL OF PHYSICAL CHEMISTRY A
A JOURNAL OF THE AMERICAN CHEMICAL SOCIETY

pubs.acs.org/JPCA
Article

Application of UHPLC-ESI-MS/MS to Identify Free Radicals via Spin Trapping with BMPO

Published as part of The Journal of Physical Chemistry A special issue "Vicki H. Grassian Festschrift".

Lena Gerritz, Véronique Perraud, Kathryn M. Weber, Manabu Shiraiwa,* and Sergey A. Nizkorodov*

Cite This: J. Phys. Chem. A 2024, 128, 10240–10249
Read Online

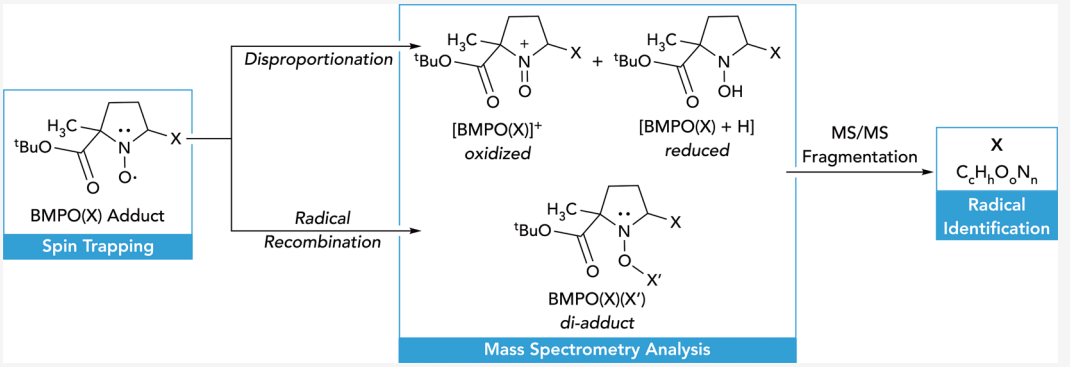

ABSTRACT: Free radicals play an important role in many chemical and biological processes, but due to their highly reactive and short-lived nature, they evade most analytical techniques, limiting our understanding of their formation and reactivity. Spin trapping molecules can react with free radicals to form radical adducts with lifetimes long enough for analysis. Mass spectrometry is an attractive way to identify radical adducts, but due to their radical nature, they form untraditional oxidized $[M]^+$ and reduced $[M+2H]^+$ ions, which complicates the interpretation of mass spectrometry analysis. This work uses simplified mixtures of radicals generated in both water and dimethyl sulfoxide (DMSO) with spin trap 5-*tert*-butoxycarbonyl-5-methyl-1-pyrroline-N-oxide (BMPO), to elucidate the behavior of nitroxide spin traps in electrospray ionization (ESI) mass spectrometry (MS) interfaced with liquid chromatography (LC). This study proposes a disproportionation mechanism to explain the formation of the oxidized and reduced BMPO adducts detected by LC-ESI-MS and explores the formation of "di-adducts" through radical recombination. We finally present a framework for differentiating between the different types of ions using collision induced fragmentation mass spectra (MS/MS). This work offers a comprehensive investigation into the behavior of radical adducts in ESI-MS to streamline the identification of organic radicals and advance understanding of radical chemistry.

INTRODUCTION

Free radicals are highly reactive, short-lived species with important chemical and biological implications. In environmental mixtures, they initiate radical chain reactions that significantly enhance the complexity of a system and often produce highly functionalized products.[1,2] Reactive oxygen species (ROS) and free radicals, including hydroxyl radical ($HO^•$), superoxide ($O_2^{-•}$), hydroperoxyl radical ($HO_2^•$), as well as a variety of organic radicals, play a central role in atmospheric multiphase processes via radical chain reactions and cyclic transformation in atmospheric chemistry.[3] They drive chemical transformation of atmospheric compounds in aerosol particles and cloud droplets, triggering the formation of secondary organic aerosols in the aqueous phase.[4,5] In the body, ROS can damage biological molecules to cause oxidative stress.[6,7] Despite the importance of free radicals in both environmental and physiological processes, understanding of their formation and reactivity is far from complete, in part due to their short lifetimes,[6] making them elusive to traditional analytical techniques.

Spin trapping compounds react with free radicals to form stable radical adducts with lifetimes on the order of minutes to hours, long enough for analysis by most analytical techniques. The most widely used class of spin traps is the nitrone family, which react via radical addition across the double bond resulting in the formation of a relatively stable oxygen centered nitroxide radical (Figure 1). Nitrones are popular due to their

Received: August 6, 2024
Revised: November 12, 2024
Accepted: November 13, 2024
Published: November 20, 2024

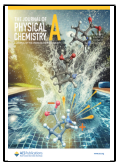

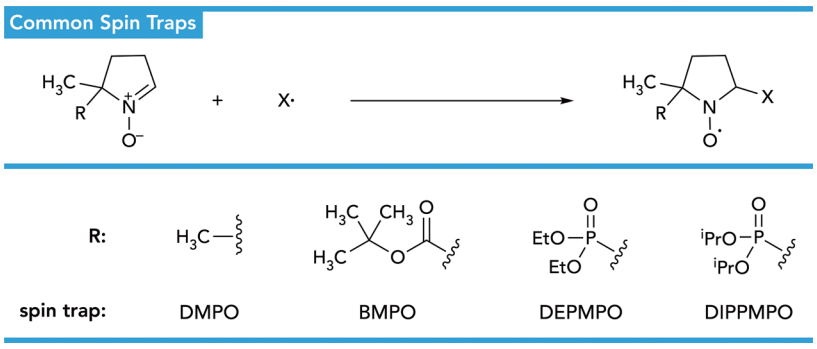

Figure 1. Nitrone spin trapping of radical X● to form a stable oxygen centered nitroxide radical adduct.

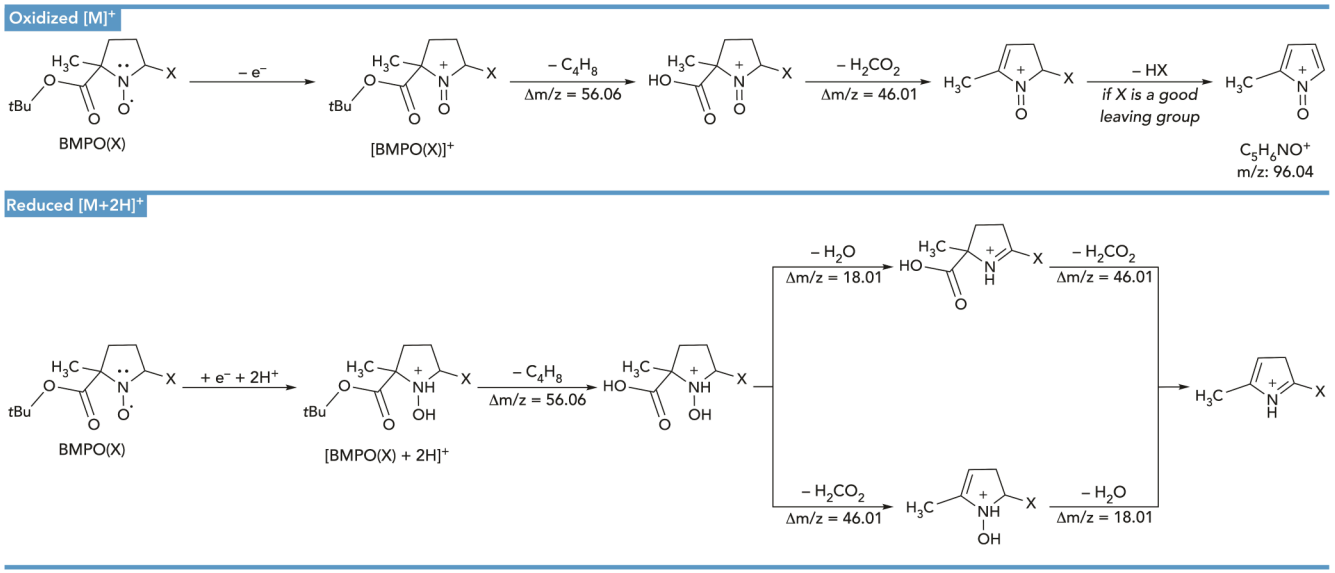

Figure 2. Fragmentation scheme for the radical adduct BMPO(X) in both its oxidized and reduced forms.

propensity to react with different types of radical species and the stability of the adducts formed.[8] The most commonly used nitrone spin trap since the 1970s has been 5,5-dimethyl-1-pyrroline-N-oxide (DMPO) and it is structurally the simplest.[9] DMPO has been shown to react slowly with the hydroperoxyl ($HO_2^{\bullet}$) and superoxide radicals ($O_2^{-\bullet}$), so since the early 2000s researchers have explored alternatives. One alternative is the spin trap featured in this work, 5-*tert*-butoxycarbonyl-5-methyl-1-pyrroline-N-oxide (BMPO), which has higher reactivity with superoxide radical and forms an adduct with a longer lifetime.[9−11]

A common technique used for radical measurements is electron paramagnetic resonance spectroscopy (EPR) that uses a magnetic field to directly detect unpaired electrons.[12,13] EPR has a time resolution of a few seconds, making it suitable for kinetic data and in situ measurements. The locations and sizes of the spectral peaks are determined by the hyperfine splitting (HFS) constants of neighboring atoms, which enables the differentiation between different types of adducts like $HO^{\bullet}$, $HO_2^{\bullet}$, carbon-centered radicals ($R^{\bullet}$), and oxygen-centered organic radicals (RO●).[12] Structural information about organic radicals is limited using EPR because the impact of HFS weakens further away from the radical site.[8] Additionally, it is difficult to identify radical adducts without previous literature on their EPR parameters. These limitations make the use of a complementary technique, such as mass spectrometry, very appealing for identifying the formulas of the radical adducts.[14−16] Recent work has described mass spectrometry derivatization methods using the stable radical molecule 2-[(2,2,6,6,-tetramethylpiperidin-1-oxyl)methyl] (TEMPO).[17] This technique has important applications in the field of peptide sequencing[18−20] and could be used for free radical identification, but the TEMPO derivatization results in a closed shell species that is no longer compatible with EPR spectroscopy. This mismatch necessitates an investigation into the behavior of EPR-active spin traps like BMPO in mass spectrometry analysis.

There are a handful of papers analyzing nitrone spin traps using electrospray ionization (ESI) mass spectrometry (MS),[21−32] but there are no publications dedicated to understanding the ion chemistry of these spin traps detected in ESI-MS. Additionally, these studies use various spin traps, radical adducts, and experimental conditions, making it difficult to directly compare their results. Previous publications include only positive ion mode data, most likely because these organic radical adducts ionize poorly in negative ion mode.[14,33] However, the nitrone spin trap adducts do not appear to produce traditional $[M+H]^+$ or $[M+Na]^+$ ions, commonly observed during electrospray ionization of closed-shell species, which necessitates in-depth investigations into the behavior of these spin traps in ESI sources. Each of the previous studies observed at least one of two major trends for nitrone-adduct

https://doi.org/10.1021/acs.jpca.4c05311
J. Phys. Chem. A 2024, 128, 10240−10249

ionization: the formation of positively charged adducts corresponding to $[M]^+$ or $[M+2H]^+$ ions. These two ionization pathways correspond to the oxidized $[M]^+$ and reduced $[M+2H]^+$ forms of the nitroxide-adduct (Figure 2), but their formation mechanisms have not been explored.[24,26] Additionally, Bauer et al.[21] suggested that the $[M+2H]^+$ pathway for DMPO occurs via a two-step process, wherein the adduct is first quenched by a hydrogen radical and then protonated during the ionization process. Similarly, Mishra et al.[34] described a derivatization method for DMPO in which excess methyl radicals generated in solution using dimethyl sulfoxide (DMSO) and Fenton chemistry recombine with radical adducts to form closed shell species that can be analyzed via gas chromatography interfaced with mass spectrometry (GC-MS). Others also observed evidence for radical recombination reactions between radical spin trap adducts and free radicals in solution contributing to the ions detected in mass spectrometry,[35−40] but do not propose a more general ionization mechanism for the formation of oxidized and reduced species.

In addition to the unconventional ionization pathways, spin trap adducts can also undergo fragmentation in the ion source,[14] further convoluting the interpretation of the mass spectrometry results. These fragmentation pathways, depend on the spin trap and adduct being studied, although the most common include ring opening[23,24,27,41] and loss of oxygen.[23,30,41] One study also observed loss of NO_2[27] and another observed loss of CO for HO adducts.[23] For BMPO, the major fragment forms through the loss of the *tert*-butyl functionality ($-C_4H_8$).[14,33] This fragmentation exposes a carboxylic acid moiety that can undergo subsequent dehydration or decarboxylation reactions, as shown in Figure 2, thus further complicating radical adduct identification.

This study investigates the ion chemistry of BMPO adducts with $HO^•$, $HO_2^•$, and organic carbon and oxygen-centered ($R^•/RO^•$) radical adducts in a heated electrospray ionization (HESI) source. We present optimized ionization parameters to minimize fragmentation products and propose a disproportionation mechanism to explain the detection of both oxidized and reduced forms of the radical adducts and discuss the products of radical recombination.

EXPERIMENTAL METHODS

Sample Preparation. Two different methods were used to generate radicals in solution. First, for the irradiated samples, 5 mM H_2O_2 (PeroxyChem, ∼30% stabilized in water) mixed with ∼10 mM BMPO (>99% Enzo Lifesciences) in ultrapure water (resistivity 18.2 MΩ-cm; total organic carbon ≤5 ppb) was irradiated for 10 min using the output of a 100 W mercury lamp filtered with a 300 nm long pass filter, as previously described.[15] Second, for the dark Fenton reactions, 0.8 M H_2O_2 and 0.08 M Fe(II), $(NH_4)_2Fe(SO_4)_2$, (Sigma-Aldrich, 99%) were used to generate HO• in a solution of ∼10 mM BMPO in DMSO (>99%) to produce organic radicals as previously described.[34,38]

UHPLC-HESI-MS/MS and Method Optimization. Analysis of BMPO and its adducts was conducted with high resolution mass spectrometry (HRMS). The mixtures (10 μL injection volume) were separated via ultrahigh performance liquid chromatography (UHPLC) using a HSS T3 Waters Acquity Premier 150 × 2.1 mm column with 1.8 μm particles. The UHPLC solvent gradient started with 95% solvent A (water acidified to pH 3 using 0.1% formic acid) and 5% solvent B (acetonitrile acidified using 0.1% formic acid) from 0 to 3 min. From 3 to 14 min, the solvent linearly increased to 95% solvent B, where it remained constant from 14 to 16 min before a linear decrease back to 95% solvent A from 16 to 22 min. Following the separation, BMPO and its adducts were detected using a Thermo Q Exactive Plus Orbitrap mass spectrometer (Thermo Scientific) equipped with a heated ESI source. The analysis was performed in ESI(+) ion mode using a full scan data-dependent MS/MS (FS-ddMS2) approach. In this approach, full MS scans were recorded over the m/z 100−1500 mass range with a resolving power of 140,000 and an automatic gain control (AGC) target of 10^6 and maximal integration time (IT) of 100 ms, while MS/MS scans were recorded for the top three most abundant ions from the adjacent full MS scan (resolving power of 17,500; AGC target, 5×10^4; max. IT, 50 ms) using normalized collision energies (NCE) of 10, 30, and 50. The starting ion source parameters were as follows: capillary temperature, 325 °C; capillary voltage, + 4.0 kV; sheath gas flow rate, 35 a. u. (arbitrary units); auxiliary gas flow rate, 10 a. u.; sweep gas flow rate, 8 a. u.; S-lens RF level 30 a. u.; auxiliary gas heater temperature, 300 °C. Negative ion mode mass spectra were also recorded but turned out to be less informative. Under these conditions, the mass spectra of BMPO and its adducts showed significant fragmentation, introducing unnecessary complexity into the data. To address this, the ionization parameters were systematically varied over the following ranges: S-lens RF (5−30), voltage (2−4), sheath gas (10−50), auxiliary gas (10−35), sweep gas (2−8), auxiliary gas temp (200−300 °C), and capillary temp (80−325 °C). Most of the parameters showed negligible improvement in the fragmentation except for capillary and auxiliary gas heater temperature which were reduced to 80 and 200 °C, respectively, in the final optimization. Note that when running solutions in DMSO the autosampler temperature was adjusted to 23 °C to prevent the samples from freezing.

The HRMS data were analyzed using Freestyle v1.3 (Thermo Scientific) to integrate the total ion chromatogram from 1.6 to 16 min to generate a raw time-integrated mass spectrum. The peak positions and relative abundances were extracted using Decon2LS software (https://omics.pnl.gov/software/decontoolsdecon2ls). Peaks containing ^{13}C, as well as peaks present in the blank at the same or greater abundances as the samples were discarded. The remaining peaks were assigned to formulas $C_cH_hO_xN_{0-2}Na_{0-1}^+$ using a mass accuracy of m/z 0.0005. Peaks with abnormal values of Kendrick mass defects (generally, above 0 for CH_2 and below 0 for O) were also removed because they were assumed to come from impurities.

RESULTS AND DISCUSSION

Notation. In this work, the term "BMPO product" refers to any species detected with a molecular formula containing at least one unit of BMPO ($C_{10}H_{17}O_3N$). The products of BMPO trapping free radicals X, as shown in Figure 1, will be referred to as "BMPO adducts" and denoted using parentheses, BMPO(X). Products that form via nonradical reactions including redox chemistry and ionization will be denoted using a plus sign according to common notation in mass spectrometry, for example, $[BMPO(X)+H]^+$, while losses due to redox chemistry or fragmentation will be denoted using a subtraction sign, for example, $[BMPO(X)-C_4H_8]^+$. In addition, when a BMPO adduct undergoes further radical recombination chemistry, it will be termed a "di-adduct" and denoted as

https://doi.org/10.1021/acs.jpca.4c05311
J. Phys. Chem. A 2024, 128, 10240−10249

$BMPO(X)_2$ and BMPO(X)(Y) depending on whether the same or different radical is trapped in the secondary step.

Electrospray Ionization Parameter Optimization. We first aimed to reduce BMPO and BMPO adduct fragmentation by adjusting the electrospray ionization parameters. Because the *tert*-butyl functional group of BMPO is thermally instable,[42] lowering the capillary temperature from 300 to 80 °C significantly increases the fraction of unfragmented protonated $[BMPO+H]^+$ ion observed at m/z 200.129 (Figure 3) that survives the ionization process, and decreases the

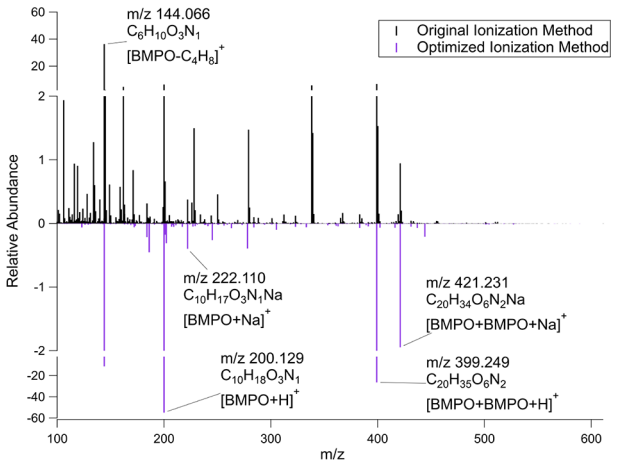

Figure 3. Normalized positive ion mode ESI mass spectra of pure BMPO in nanopure water with the original ESI ionization method (black) and the optimized lower temperature ionization method (purple). Peaks of $[BMPO+H]^+$ (m/z 200.129), $[BMPO+Na]^+$ (m/z 222.110), $[BMPO+BMPO+H]^+$ (m/z 399.249) and $[BMPO+BMPO+Na]^+$ (m/z 421.231) are labeled with ion formulas in the bottom panel. The peak at m/z 144.066 corresponds to $[C_6H_{10}O_3N]^+$, a major fragment of BMPO ionization ($[BMPO-C_4H_8]^+$), which is considerably reduced after the optimization of the capillary temperature, and the mass spectrum on the whole becomes cleaner. Note that peaks corresponding to ^{13}C isomers were removed during processing.

fraction of the $[BMPO-C_4H_8]^+$ fragment ion. The lower temperature also reduces the amount of additional fragmentation to negligible abundances, as evidenced by the disappearance of peaks below m/z 144 in Figure 3. For example, when the *tert*-butyl group is removed, BMPO is left with an exposed carboxylic acid group which is expected to undergo further fragmentation through loss of a H_2CO_2 group (Figure 2).[43,44]

The decrease in temperature slightly increases the relative abundance of the $[BMPO+BMPO+H]^+$ and $[BMPO+BMPO+Na]^+$ cluster ions at m/z 399.249 and 421.231, respectively, which is expected as it is more entropically favorable for large clusters to break apart at higher temperatures. Although this increase in clustering slightly detracts from the signal of native BMPO molecules detected, the signal at m/z 200.129 is abundant enough that the clustering does not introduce detection limitations. When multiple BMPO adducts are present, the benefit of minimizing ion fragmentation outweighs the disadvantage of having some cluster ions in the mass spectrum. Additionally, the clusters formed using the optimized parameters are easy to recognize because they have higher m/z values compared to most BMPO adducts of interest in our systems, and their formulas contain two BMPO units. Overall, it is much easier to account for the effects of clustering on the mass spectra than fragmentation by often unknown mechanisms.

BMPO(OH) and BMPO(OOH) Adducts. Figure 4 shows a portion of the positive ion mode mass spectrum of irradiated

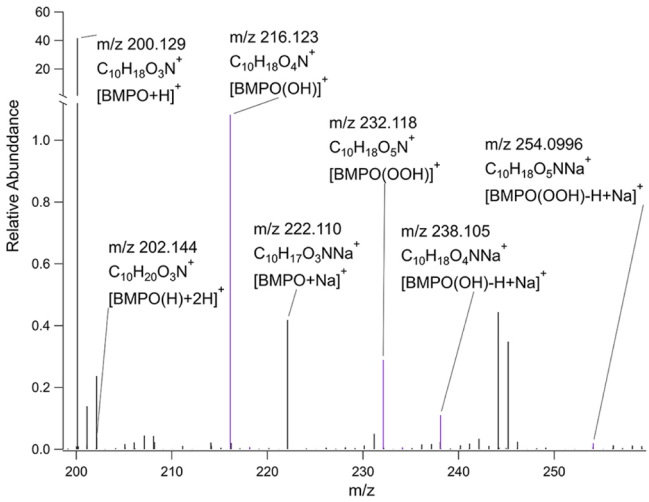

Figure 4. Normalized positive ion mode mass spectra of irradiated BMPO + H_2O_2 solution, zoomed in from m/z 200 to 260. Peaks with selected ion chromatograms shown in Figure 5 are highlighted in purple. An extended mass spectra (m/z 100–650) is presented in Figure S1. Note that peaks corresponding to ^{13}C isomers were removed during processing.

H_2O_2 and BMPO obtained by integration of the chromatogram over 1.6–16 min (the complete positive ion mode mass spectrum can be seen in Figure S1). The most abundant peak at m/z 200.129 corresponds to $[BMPO+H]^+$ while the peak at m/z 222.110 corresponds to $[BMPO+Na]^+$, as previously described. Instead of being detected as a protonated ion, the BMPO(OH) adduct is observed at m/z 216.123 and 238.105 for $[M]^+$ and $[M-H+Na]^+$, respectively, and the BMPO(OOH) adduct appears primarily at m/z 232.118 ($[M]^+$) with only a minor contribution at m/z 254.0996 ($[M-H+Na]^+$).

Figure 5 shows the total ion chromatogram (TIC, panel A) for the irradiated H_2O_2 mixture as well as selected ion chromatograms (SICs) for BMPO(OH) (panel B) and BMPO(OOH) (panel C) ions corresponding to $[M]^+$, $[M-H+Na]^+$, and $[M+2H]^+$ products. As evidenced by the relative intensities in Figure 5, both HO• and HO_2• radicals predominantly form the oxidized $[M]^+$ product, but the reduced $[M+2H]^+$ pathway becomes important for larger BMPO adducts discussed later so it is included in the figure.

For both BMPO(OH) and BMPO(OOH) the SICs for $[M]^+$ and $[M-H+Na]^+$ contain peaks at the same retention times, which suggest it is the same product that ionizes differently in the ion source. In stark contrast to this, the chromatograms for the $[M+2H]^+$ pathway are distinctly different, suggesting chemically distinct species formed *before* the LC separation. The number of peaks also varies across the different SICs, suggesting the presence of multiple isomers, and this will be further explored in the discussion section.

BMPO(R) Adducts. Figure S2 shows the full mass spectrum of the products from the HO• oxidation of DMSO in the presence of BMPO. This oxidation produces several organic radicals that are spin trapped by BMPO enabling their identification via HRMS. Figure 6 shows a closer view of the mass spectrum focusing on m/z 210–250 range only, with

https://doi.org/10.1021/acs.jpca.4c05311
J. Phys. Chem. A 2024, 128, 10240–10249

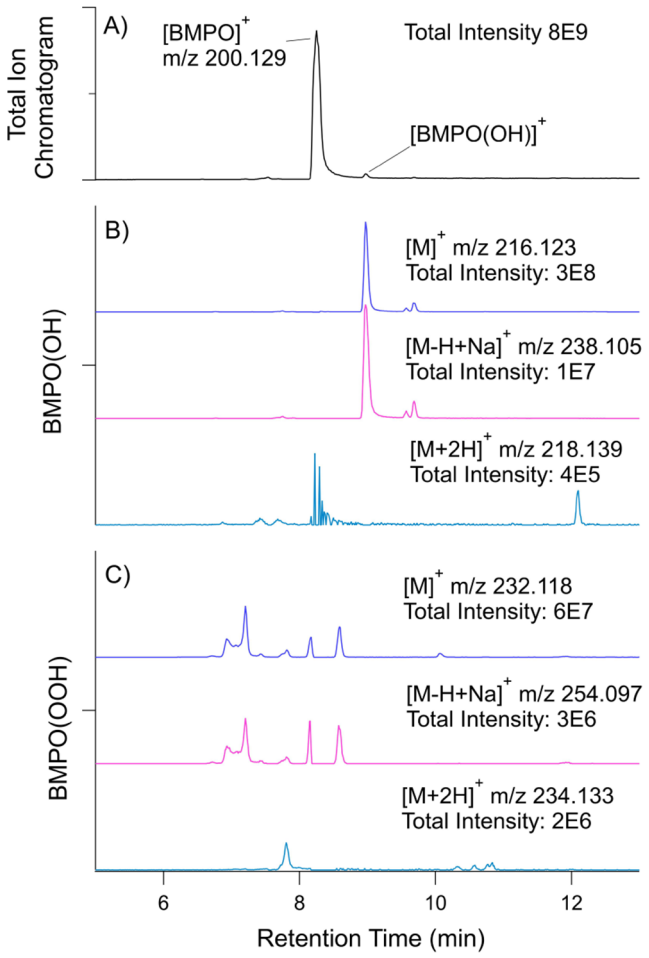

Figure 5. Total ion chromatogram (panel A) for the irradiated H_2O_2 + BMPO mixture and selected ion chromatograms for BMPO(OH) (panel B) and BMPO(OOH) (panel C) ions for $[M]^+$ (purple), $[M-H+Na]^+$(pink), and $[M+2H]^+$(blue) ionization pathways. The intesities refer to the total ion current for the selected ion chromatogram across all retention times. The chromatograms shown here were normalized to their total intensity across 1.6−16 min for qualitative comparison.

highlighted peaks corresponding to three major BMPO products with formulas indicating the apparent addition of CH_3, CH_3O, and C_2H_5. Both $\bullet CH_3$ and $\bullet CH_3O$ are well-known to form via the reaction of hydroxyl radicals and DMSO,[38] and these adducts are detected as both the $[M]^+$ ions and the $[M+2H]^+$ ions at m/z 214.114 and 216.160, and m/z 230.139 and 232.154, respectively. The BMPO(CH_3) preferentially ionizes in its oxidized form with a relative abundance over 250 times higher than its reduced form while BMPO(CH_3O) is detected in its reduced form about 5 times more than its oxidized form. This suggests that the identity of the radical adduct strongly affects the distribution of oxidation products formed. The most abundant ion highlighted in Figure 6 corresponds to the apparent addition of C_2H_5 to BMPO at m/z 228.160 and m/z 230.175, but ethyl radical is not an expected product of DMSO oxidation. This suggests BMPO $+C_2H_5$ does not form by the direct trapping of an ethyl radical, but instead it forms via the radical recombination of a BMPO(CH_3) adduct with another methyl radical forming a closed shell species (Figure S3, BMPO$(CH_3)_2$) as described by

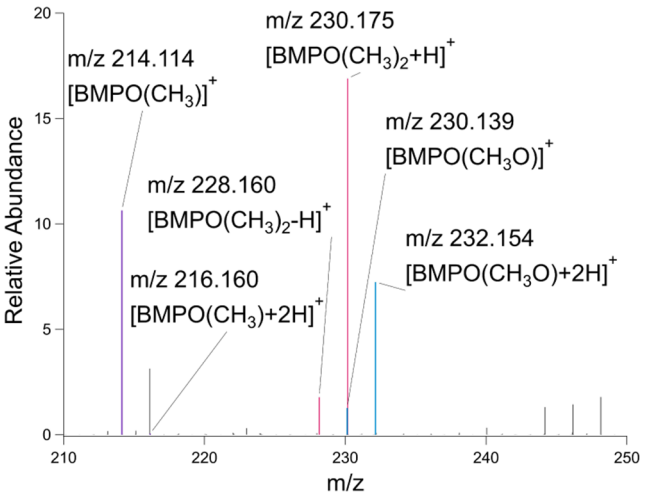

Figure 6. Normalized positive ion mode mass spectrum of the dark Fenton reaction between Fe(II) and H_2O_2 in DMSO with 10 mM BMPO from m/z 100−250 and spectrum with highlighted contributions from CH_3 adduct (purple), $(CH_3)_2$ diadduct (pink), and CH_3O adduct (blue). An extended mass spectra (m/z 100−350) is presented in Figure S2. Note that peaks corresponding to ^{13}C isomers were removed during processing.

Mishra et al.[34] This is discussed further below with support from MS/MS analysis.

The TIC and SICs for BMPO adducts with CH_3 and CH_3O in both their oxidized ($[M]^+$) and reduced ($[M+2H]^+$) ions are shown in Figure 7 along with the $[M-H]^+$ and $[M+H]^+$ ions for BMPO$(CH_3)_2$ diadduct. The $[M-H+Na]^+$ pathway for the organic radical adducts has a very low relative abundance, so it is not included in the SIC. For all three of these products, the retention times of major peaks are different for the $[M]^+$ and $[M+2H]^+$ SICs. This is similar to the observations made for BMPO(OH) and BMPO(OOH) adducts, suggesting that precursors of $[M]^+$ and $[M+2H]^+$ ions are chemically distinct.

Discussion of Nitroxide Radical Chemistry. Nitroxide radicals are known to decay by several mechanisms including disproportionation.[45−48] Figure 8 shows an example of acid-catalyzed disproportionation between two BMPO(X) radicals, resulting in the formation of a positively charged oxidized species with the same formula as the initial BMPO(X) radical ($[M]^+$) and a neutral reduced species with an extra hydrogen atom ($[M+2H]^+$). Disproportionation could also occur between any two radicals interacting in the solution where disproportionation is favored. These products are not unique to BMPO and have been shown for other types of nitroxides,[21,24−27,29−32,37] suggesting our findings offer an explanation for a wider variety of spin trapping experiments. For example, TEMPO and its derivatives have been shown to undergo this disproportionation to generate both the oxidized and reduced forms,[45,47−49] and recent work actually recommends converting all TEMPO related species in a sample to the reduced form prior to LCMS analysis.[50] Although this method is more rigorous for quantification, we avoided introducing any additional variables into the system that may alter the radical chemistry, and chose not to add this step to our sample preparation. Additionally, as shown in Figure 8, we hypothesize that the acidic conditions employed for the mobile phase catalyze disproportionation, thus promoting conversion into oxidized and reduced forms of the BMPO adducts prior to ionization. We expect the oxidized and reduced forms of the

https://doi.org/10.1021/acs.jpca.4c05311
J. Phys. Chem. A 2024, 128, 10240−10249

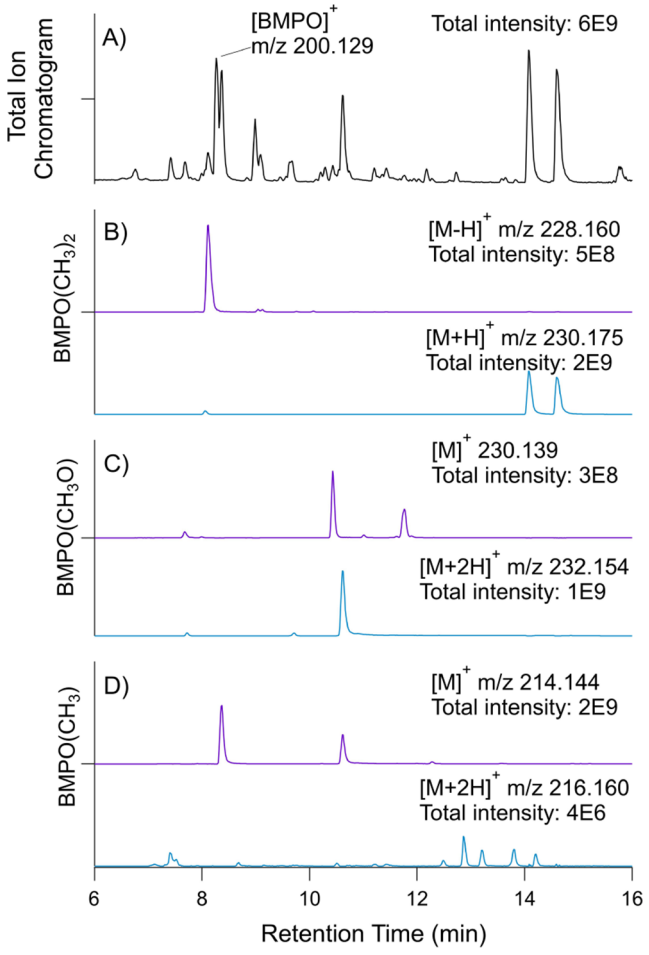

Figure 7. Total ion chromatogram, excluding m/z 157 DMSO contamination peak, (panel A) for the irradiated H_2O_2 + BMPO in DMSO mixture and selected ion chromatograms for $BMPO(CH_3)_2$ (Panel B), $BMPO(CH_3O)$ or $BMPO(OH)(CH_3)$ (Panel C), and $BMPO(CH_3)$ (Panel D) ions for $[M]^+$ or $[M\text{-}H]^+$ (purple) and $[M+2H]^+$ or $[M+H]^+$ (blue) ionization pathways. The intesities refer to the total ion current for the selected ion chromatogram across all retention times. The chromatograms shown here were normalized to their total intensity across 1.6−16 min for qualitative comparison.

BMPO adducts to form rapidly upon mixing with the acidic mobile phase (which has pH ∼ 3), which explains the differences in the retention times for the different adducts. The oxidized form is already positively charged, promoting early elution from the column between 7 and 10 min, and corresponds to the $[M]^+$ signal observed, while the reduced form has a neutral mass of (M+H), leading to the detection of an $[M+2H]^+$ ion after ionization. It has been shown that the identity of the adduct can affect the rate and reversibility of disproportionation as well as the protonation efficiency.[49] These findings can help explain the variation in retention times and relative abundance of the oxidized and reduced forms for different radical adducts.

Radical Recombination. In addition to disproportionation, radicals can also undergo recombination to form a closed shell species, as described by Mishra et al.,[34] depending on the stability of the products and the abundance of radical species in the mixture. The radical recombination of two large radicals such as BMPO adducts would be highly sterically hindered and entropically unfavorable, so these interactions are more likely to result in disproportionation, forming one oxidized and one reduced species. However, recombination of a BMPO adduct with a smaller radical is feasible and often favorable, as described by a computational study by Boyd and Boyd (1994),[40] and we observe evidence for radical recombination in our mass spectra. We propose that this radical recombination is responsible for the high abundance of the $BMPO(CH_3)_2$ diadduct in Figure 6. This double addition of $\bullet CH_3$ to BMPO, is supported by the MS/MS fragmentation spectra of the peaks at m/z 228.160 and 230.175, shown in Figure S4, corresponding to the $[M\text{-}H]^+$ and the $[M+H]^+$ forms of the $BMPO(CH_3)_2$ diadduct, respectively. Proposed fragmentation pathways based on the m/z detected by MS are shown in Figure S3. The largest peak in each spectrum of Figure S4 (m/z 172.097 and 174.113, respectively) corresponds to the loss of the *tert*-butyl group (C_4H_8), typical of BMPO fragmentation as previously discussed. The next largest fragmentation peak for m/z 228.160 (Figure S4A) at m/z 96.081 corresponds to the loss of $C_2H_4O_3$ from m/z 172.097 attributed to the loss of the carboxylic acid group as H_2CO_2 along with CH_2O, suggesting the presence of a methoxy functional group that would be formed via radical recombination of $BMPO(CH_3)$ and a methyl radical. Similarly, the next largest fragmentation peak for m/z 230.175 (Figures S4B,C) is m/z 128.107, suggesting the loss of H_2CO_2 corresponding to the loss of the carboxylic acid group, while a small fragmentation peak at m/z 142.087 corresponds to the loss of CH_3OH from the BMPO adduct, consistent with the methoxy functional group. The other peaks at m/z 98.096 and 96.081 correspond to the loss of $C_2H_4O_3$ and $C_2H_6O_3$ from the fragment at m/z 174.113, respectively both of which can be explained by the loss of a carboxylic acid group followed by the loss of a methoxy functional group. The observed MS/MS fragmentation peaks in Figure S4 agree with the fragmentation mechanism predicted in Figure S3 for both the $[M\text{-}H]^+$ and $[M + H]^+$ ions of $BMPO(CH_3)_2$ diadduct.

In Figure 7C, two apparent $BMPO(CH_3O)$ isomers are observed at RT 10.4 and 11.7 min, respectively. The fragmentation spectra for m/z 230.139, shown in Figures S5A,B, indicate that the isomer eluting 10.4 min is the $[M]^+$ for

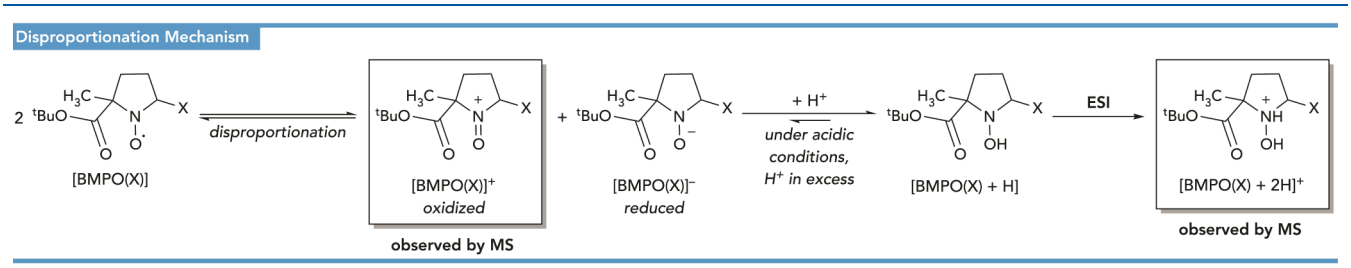

Figure 8. Acid-catalyzed disproportionation mechanism for radical adduct BMPO(X) followed by ionization for the neutral reduced species.

https://doi.org/10.1021/acs.jpca.4c05311
J. Phys. Chem. A 2024, 128, 10240−10249

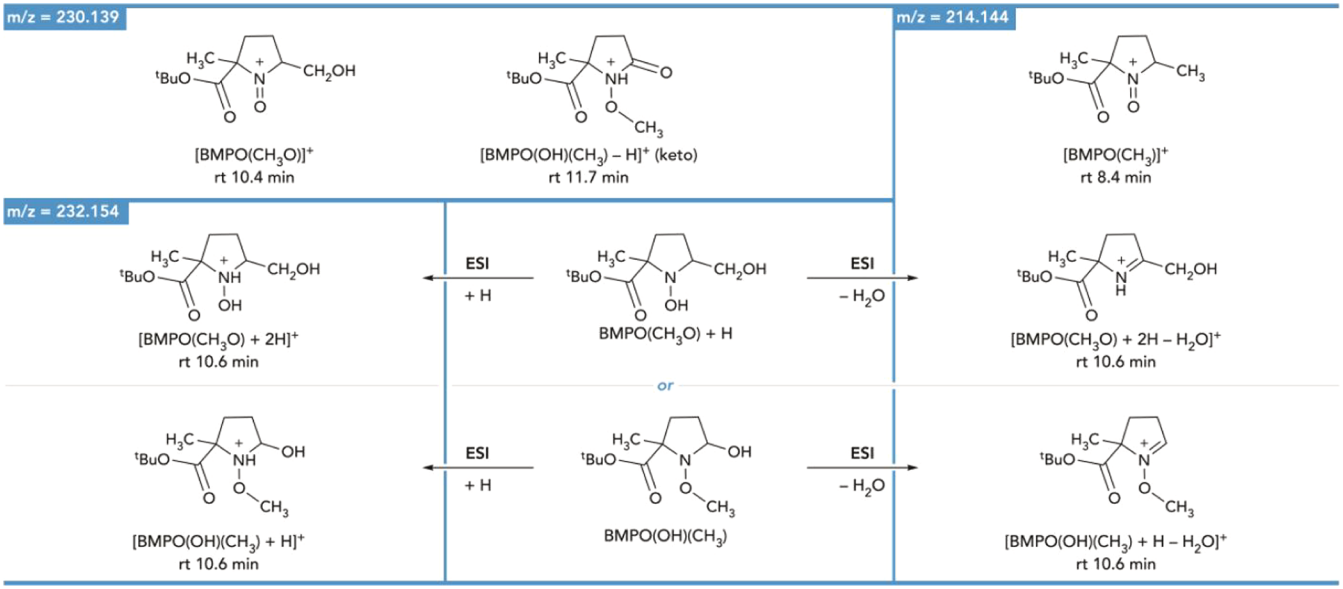

Figure 9. Proposed structures for BMPO(R) organic radicals based on the MS/MS fragmentation spectra. Clockwise from top left corner: m/z 230.139 products $[BMPO(CH_3O)]^+$ with RT 10.4 min and the keto tautomer of $[BMPO(OH)(CH_3)\text{-}H]^+$ at 11.7 min; m/z 214.144 product $[BMPO(CH_3)]^+$ at RT 8.4 min and the fragmentation product at 10.6 min produced by the loss water from m/z 232.154 either $[BMPO(CH_3O)+2H]^+$ or $[BMPO(OH)(CH_3)+H]^+$ at 10.6 min. Note that the structure for m/z 230.139 at 11.7 min is expected to be the keto tautomer, a neutral species, to explain the later retention time.

$BMPO(CH_3O)$ while the isomer at 11.7 min is likely a $BMPO(OH)(CH_3)$ diadduct, as depicted in Figure 9. The fragmentation mass spectrum at 10.4 min, shown in Figure S5A, only contains two major peaks at m/z 174.076 and m/z 128.071 corresponding to the loss of *tert*-butyl and subsequent carboxylic acid group, respectively. This is consistent with the expected fragmentation of oxidized BMPO $[M]^+$ adducts shown in Figure 2. These are also the largest peaks for the isomer at 11.7 min, but this fragmentation spectrum, Figure S5B, contains additional peaks. The fragment at m/z 112.076 is formed via the loss of a H_2CO_3, likely as the loss of H_2O and CO_2 in rapid succession from the m/z 174.076 fragment. Furthermore, the peak at m/z 84.081 can be explained by the subsequent loss of CO from the nitroxide adduct at m/z 112.076. The loss of every oxygen from the original structure is uncharacteristic of oxidized BMPO adducts as they contain a double bond between the N and O, which is not easily fragmented, suggesting the presence of a radical recombination for this isomer. There is an additional major peak in this fragmentation spectrum at m/z 102.055 with the molecular formula $C_4H_8O_2N^+$, which is not observed in any other fragmentation spectra. We suspect this fragment is formed via a ring opening mechanism similar to those previously described.[24,41] As this fragment is only observed for one ion, its fragmentation mechanism is not described further so as to focus our attention on the more generalizable fragmentation patterns that assist in the identification of different types of BMPO products. The additional fragmentation products suggest the isomer of m/z 230.139 at 11.7 min is a diadduct produced by the recombination of BMPO(OH) with a methyl radical while the isomer at 10.4 min is consistent with the oxidized ion of $BMPO(CH_3O)$ adduct. There is only one isomer observed in the SIC for m/z 232.154 shown in Figure 7C and due to similarities in the functional groups, we are unable to conclusively differentiate the $BMPO(CH_3O)$ $[M+2H]^+$ adduct from a $BMPO(OH)(CH_3)$ diadduct $[M+H]^+$ based solely on the MS/MS data.

The SIC for $[BMPO(CH_3)]^+$ (m/z 214.144) (Figure 7D) contains two peaks at 8.4 and 10.6 min with different fragmentation mass spectra shown in Figure S6, suggesting two structural isomers shown in Figure 9. The MS/MS of the 8.4 min isomer (Figure S6A) shows a major fragment at m/z 158.081, which corresponds to the loss of the *tert*-butyl and a less abundant peak at m/z 112.076 corresponding to the subsequent loss of H_2CO_2, both of which are consistent with the expected fragmentation of oxidized adducts detailed in Figure 2. We suspect the isomer of m/z 214.144 at RT 10.6 min is a fragment of the reduced $BMPO(CH_3O)$ species, shown in Figure 9, due their identical retention times (Figure 7) and the presence of a fragment at m/z 214.144 in the MS/MS of $[BMPO(CH_3O)+2H]^+$, shown in Figure S5C. Additionally, the MS/MS for the isomer of m/z 214.144 at RT 10.6 in Figure S6B contains the same major peaks as the MS/MS for m/z 232.154 Figure S5C, with the exception of the peak at m/z 176.092. This further supports that this isomer of m/z 214.144 is produced via the fragmentation of m/z 232.154 and is attributed to the ESI fragment of $BMPO(CH_3O)$ adduct. The relative intensity for the $[BMPO(CH_3)+2H]^+$ SIC is significantly lower than that of the $[M]^+$ form, suggesting this is not a major ion formed for this adduct. The multitude of peaks in the SIC may be explained by contributions from fragmentation products of larger BMPO adducts but given the low relative intensity we are not going to discuss this ion further.

We also propose that the radical recombination of HO• with BMPO(OH) (forming a $BMPO(OH)_2$ diadduct) is responsible for some of the isomers detected at m/z 232.118 on the SICs chromatograms shown in Figure 5C. In the case of recombination, the apparent $[M]^+$ ion observed at m/z 232.118 would correspond to the $[M\text{-}H]^+$ ion of the diadduct instead, while the apparent $[M+2H]^+$ ion would correspond to

https://doi.org/10.1021/acs.jpca.4c05311
J. Phys. Chem. A 2024, 128, 10240−10249

its $[M+H]^+$ form. In addition, the disproportionation of BMPO(OOH) is expected to produce two diastereomers via addition over the double bond. Diastereomers can sometimes be separated via liquid chromatography,[51] but this would only explain the appearance of two peaks in the chromatogram, as opposed to at least four peaks observed for BMPO (OOH) in Figure 5C. The additional peaks suggest the formation of additional structural isomers of $[C_{10}H_{18}O_5N]^+$, which may be explained by the radical recombination of BMPO(OH) radical adduct with an HO• radical. This is further supported by differences between the MS/MS fragmentation spectra at different retention times shown in Figure S7, but the fragmentation patterns do not provide enough information to conclusively identify the molecular structures responsible for the different peaks. Based on the appearance of these isomers, we suspect that hydroxyl radical undergoes radical recombination with BMPO adducts, but the computational work by Boyd and Boyd indicates that this reaction is less favored than the formation of two BMPO(OH) mono radical adducts, so it is not expected to be the primary product formed.[40] It is also possible for a HO• and a BMPO adduct to undergo disproportionation forming an oxidized $[BMPO(OH)]^+$ and a reduced OH^-, which would help explain the dominance of the oxidized BMPO adducts in solutions with excess HO•. Further computational work would be helpful in determining the branching ratios of these radical quenching reactions.

Generalized MS/MS Approach for Spin Trap Adduct Identification. The expected fragmentation of the oxidized and reduced ions generalized for a BMPO(X) adduct proposed in Figure 2 are based off literature fragmentation pathways[44,52] and supported by the MS/MS fragmentation spectra of $[BMPO(OH)]^+$ and $[BMPO(H)+2H]^+$, Figures S8 and S9, respectively. Regardless of oxidation state, all BMPO derivatives fragment via the loss of a *tert*-butyl functional group ($-C_4H_8$), as discussed in the optimization section. This results in an exposed carboxylic acid functional group which can be lost as either H_2CO_2 or CO_2.[43,44,52] When a BMPO adduct is in its reduced state or undergoes radical recombination to form a larger functional group on the oxygen in the nitroxide to form a secondary hydroxylamine with a relatively weak N−O single bond that is more easily lost during fragmentation. This results in a characteristic additional loss of water for reduced molecules, as demonstrated in the MS/MS spectrum for $[BMPO(H)+2H]^+$ m/z 202.144, shown in Figure S8, or the loss of an O-R group for a BMPO(R) adduct that has undergone radical recombination with another free radical R•, as seen in the fragmentation of $BMPO(CH_3)_2$ ions in Figures S4 and S3. Oxidized BMPO adducts contain an N = O moiety, so the fragmentation spectra generally consist only of a loss of the *tert*-butyl molecule and H_2CO_2, as shown for $[BMPO(OH)]^+$ in Figure S9 and $[BMPO(CH_3)]^+$ in Figure S7. Oxidized, reduced, and recombined ions can undergo additional fragmentation if the radical adduct contains functional groups that can be favorably lost at the high energies applied during collision induced dissociation.

The examination of MS/MS spectra can provide useful information for identifying the trapped radicals, unless the radical adduct, X, and the O-R group formed during radical recombination have identical ion structures as in the case of BMPO(OOH) ($[M]^+$) and $BMPO(OH)_2$ ($[M-H]^+$). In this case, we advise against using mass spectrometry for the identification of spin trapped radical adducts. Fortunately, BMPO(OH) and BMPO(OOH) can be identified using EPR so it is not essential to resolve them using mass spectrometry. This ambiguity was also present for reduced $BMPO(CH_3O)$ product at m/z 232.154 (Figure S5C), but the oxidized $[M]^+$ data was differentiable, so we were still able to identify both the adduct and diadduct in the sample. Additionally, we expect less diadduct formation in more complex samples because they are typically designed with excess BMPO to promote radical trapping while the experiments in this work generated an excess of radicals. In our previous work with more complex mixtures,[14,15] we observed no substantial diadduct formation, but we were unable to differentiate between the oxidized and reduced radical adducts, leading to uncertainty in our adduct identifications. In future experiments this uncertainty can be reduced using MS/MS data to differentiate between oxidized and reduced BMPO adducts.

CONCLUSIONS

The presence of oxidized, reduced, and diadduct species greatly complicates the use of mass spectrometry to identify BMPO radical adducts, especially in the case of complex mixtures. This analysis demonstrates that the identity of radical adducts cannot simply be deduced from the additions to the molecular formula of BMPO ($C_{10}H_{17}O_3N$), as the oxidized and reduced forms introduce uncertainty in the number of hydrogens in the adduct and recombination muddles the identity of a single radical adduct with the formation of a diadduct. However, examination of the MS/MS spectra for major ions reveals several trends that can be useful in elucidating whether a BMPO adduct has undergone oxidation, reduction, or recombination prior to mass spectrometry analysis.

Although this work only examined the mass spectrometry of BMPO and its adducts, we expect most of these findings to be generalizable to the behavior of other nitroxide radical spin traps in ESI as supported by the previous studies observing similar behavior for other spin traps.[23−27,30,31,53,54] For example, the most widely used spin trap, DMPO, is structurally the same as BMPO with the *tert*-butoxycarbonyl functional group replaced by a methyl group. This difference in structure likely simplifies the fragmentation of DMPO in ESI and we would only expect to see the loss of water from a reduced ions or the loss of an easily fragmented radical adduct. We otherwise believe the analysis presented here can also be extended to DMPO radical adducts. This work serves as a roadmap for organic radical identification using a variety of nitroxide spin traps for future work.

ASSOCIATED CONTENT

Supporting Information

The Supporting Information is available free of charge at https://pubs.acs.org/doi/10.1021/acs.jpca.4c05311.

Extended mass spectra for Figure 4 from m/z 100−650; extended mass spectra for Figure 6 from m/z 100−650; formation and fragmentation pathway for $BMPO(CH_3)_2$; fragmentation mass spectra for $BMPO(CH_3)_2$ nitroxide adduct (m/z 228.160 and 230.175 in Figure 6); fragmentation mass spectra for $BMPO(CH_3O)$ and $BMPO(OH)(CH_3)$ nitroxide adducts (m/z 230.139 and 232.154 in Figure 6); fragmentation mass spectra for $BMPO(CH_3)$ nitroxide adduct (m/z 214.144 in Figure 6); fragmentation mass spectra for BMPO(OOH) and $BMPO(OH)_2$ nitroxide adducts (m/z 232.118 in Figure

https://doi.org/10.1021/acs.jpca.4c05311
J. Phys. Chem. A 2024, 128, 10240−10249

4); fragmentation mass spectra for $[BMPO(H)+2H]^+$ (m/z 202.144 in Figure 4); and fragmentation mass spectra for $[BMPO(OH)]^+$ (m/z 216.123 in Figure 4) (PDF)

AUTHOR INFORMATION

Corresponding Authors

Manabu Shiraiwa − *Department of Chemistry, University of California, Irvine, California 92697, United States;* orcid.org/0000-0003-2532-5373; Email: m.shiraiwa@uci.edu

Sergey A. Nizkorodov − *Department of Chemistry, University of California, Irvine, California 92697, United States;* orcid.org/0000-0003-0891-0052; Email: nizkorod@uci.edu

Authors

Lena Gerritz − *Department of Chemistry, University of California, Irvine, California 92697, United States;* orcid.org/0009-0009-9971-1526

Véronique Perraud − *Department of Chemistry, University of California, Irvine, California 92697, United States;* orcid.org/0000-0003-1247-9787

Kathryn M. Weber − *Department of Chemistry, University of Wisconsin, Madison, Wisconsin 53706, United States*

Complete contact information is available at: https://pubs.acs.org/10.1021/acs.jpca.4c05311

Author Contributions

M.S. and S.A.N. advised on the experiments, L.G. did the experiments and wrote the manuscript, V.P. designed parameter optimization experiments and assisted with data interpretation, K.M.W. proposed the chemical mechanisms. All authors contributed to editing the manuscript.

Notes

The authors declare no competing financial interest.

ACKNOWLEDGMENTS

The authors thank the National Science Foundation grant CHE-2203419 for supporting this work. L.G. thanks the NSF-GRFP program for supporting her research. The authors thank Dr. Lisa Wingen for her help with the high-resolution mass spectrometry measurements.

REFERENCES

(1) Lim, Y. B.; Tan, Y.; Perri, M. J.; Seitzinger, S. P.; Turpin, B. J. Aqueous Chemistry and Its Role in Secondary Organic Aerosol (SOA) Formation. *Atmos. Chem. Phys.* **2010**, *10* (21), 10521−10539.

(2) Huang, L.; Liu, T.; Grassian, V. H. Radical-Initiated Formation of Aromatic Organosulfates and Sulfonates in the Aqueous Phase. *Environ. Sci. Technol.* **2020**, *54* (19), 11857−11864.

(3) Pöschl, U.; Shiraiwa, M. Multiphase Chemistry at the Atmosphere−Biosphere Interface Influencing Climate and Public Health in the Anthropocene. *Chem. Rev.* **2015**, *115* (10), 4440−4475.

(4) Ervens, B.; Turpin, B. J.; Weber, R. J. Secondary Organic Aerosol Formation in Cloud Droplets and Aqueous Particles (aqSOA): A Review of Laboratory, Field and Model Studies. *Atmos. Chem. Phys.* **2011**, *11* (21), 11069−11102.

(5) McNeill, V. F. Aqueous Organic Chemistry in the Atmosphere: Sources and Chemical Processing of Organic Aerosols. *Environ. Sci. Technol.* **2015**, *49* (3), 1237−1244.

(6) Sies, H.; Berndt, C.; Jones, D. P. Oxidative Stress. *Annu. Rev. Biochem.* **2017**, *86* (1), 715−748.

(7) Shiraiwa, M.; Ueda, K.; Pozzer, A.; Lammel, G.; Kampf, C. J.; Fushimi, A.; Enami, S.; Arangio, A. M.; Frohlich-Nowoisky, J.; Fujitani, Y.; Furuyama, A.; et al. Aerosol Health Effects from Molecular to Global Scales. *Environ. Sci. Technol.* **2017**, *51* (23), 13545−13567.

(8) Buettner, G. R. Spin Trapping: ESR Parameters of Spin Adducts 1474 1528V. *Free Radical Biol. Med.* **1987**, *3* (4), 259−303.

(9) Tsai, P.; Ichikawa, K.; Mailer, C.; Pou, S.; Halpern, H. J.; Robinson, B. H.; Nielsen, R.; Rosen, G. M. Esters of 5-Carboxyl-5-Methyl-1-Pyrroline *N* -Oxide: A Family of Spin Traps for Superoxide. *J. Org. Chem.* **2003**, *68* (20), 7811−7817.

(10) Zhao, H.; Joseph, J.; Zhang, H.; Karoui, H.; Kalyanaraman, B. Synthesis and Biochemical Applications of a Solid Cyclic Nitrone Spin Trap: A Relatively Superior Trap for Detecting Superoxide Anions and Glutathiyl Radicals. *Free Radical Biol. Med.* **2001**, *31* (5), 599−606.

(11) Wei, J.; Fang, T.; Shiraiwa, M. Effects of Acidity on Reactive Oxygen Species Formation from Secondary Organic Aerosols. *ACS Environ. Au* **2022**, *2* (4), 336−345.

(12) Roessler, M. M.; Salvadori, E. Principles and Applications of EPR Spectroscopy in the Chemical Sciences. *Chem. Soc. Rev.* **2018**, *47* (8), 2534−2553.

(13) Villamena, F. A. EPR Spin Trapping. In *Reactive Species Detection in Biology*; Elsevier, 2017; pp. 163−202.

(14) Gerritz, L.; Schervish, M.; Lakey, P. S. J.; Oeij, T.; Wei, J.; Nizkorodov, S. A.; Shiraiwa, M. Photoenhanced Radical Formation in Aqueous Mixtures of Levoglucosan and Benzoquinone: Implications to Photochemical Aging of Biomass-Burning Organic Aerosols. *J. Phys. Chem. A* **2023**, *127* (24), 5209−5221.

(15) Gerritz, L.; Wei, J.; Fang, T.; Wong, C.; Klodt, A. L.; Nizkorodov, S. A.; Shiraiwa, M. Reactive Oxygen Species Formation and Peroxide and Carbonyl Decomposition in Aqueous Photolysis of Secondary Organic Aerosols. *Environ. Sci. Technol.* **2024**, *58* (10), 4716−4726.

(16) Tong, H.; Arangio, A. M.; Lakey, P. S. J.; Berkemeier, T.; Liu, F.; Kampf, C. J.; Brune, W. H.; Pöschl, U.; Shiraiwa, M. Hydroxyl Radicals from Secondary Organic Aerosol Decomposition in Water. *Atmos. Chem. Phys.* **2016**, *16* (3), 1761−1771.

(17) Lee, S. T.; Park, H.; Jang, I.; Lee, C. S.; Moon, B.; Oh, H. B. New Free Radical-Initiated Peptide Sequencing (FRIPS) Mass Spectrometry Reagent with High Conjugation Efficiency Enabling Single-Step Peptide Sequencing. *Sci. Rep.* **2022**, *12* (1), 9494.

(18) Lee, M.; Kang, M.; Moon, B.; Oh, H. B. Gas-Phase Peptide Sequencing by TEMPO-Mediated Radical Generation. *Analyst* **2009**, *134* (8), 1706.

(19) Marshall, D. L.; Hansen, C. S.; Trevitt, A. J.; Oh, H. B.; Blanksby, S. J. Photodissociation of TEMPO-Modified Peptides: New Approaches to Radical-Directed Dissociation of Biomolecules. *Phys. Chem. Chem. Phys.* **2014**, *16* (10), 4871.

(20) Lee, M.; Lee, Y.; Kang, M.; Park, H.; Seong, Y.; June Sung, B.; Moon, B.; Bin Oh, H. Disulfide Bond Cleavage in TEMPO-free Radical Initiated Peptide Sequencing Mass Spectrometry. *J. Mass Spectrom.* **2011**, *46* (8), 830−839.

(21) Bauer, N. A.; Hoque, E.; Wolf, M.; Kleigrewe, K.; Hofmann, T. Detection of the Formyl Radical by EPR Spin-Trapping and Mass Spectrometry. *Free Radical Biol. Med.* **2018**, *116*, 129−133.

(22) Domingues, P.; Fonseca, C.; Reis, A.; Domingues, M. R. M. Identification of Isomeric Spin Adducts of Leu-Tyr and Tyr-Leu Free Radicals Using Liquid Chromatography-Tandem Mass Spectrometry: LC-MSn of DMPO Adducts of Tyr-Leu and Leu-Tyr Radicals. *Biomed. Chromatogr.* **2012**, *26* (1), 51−60.

(23) Domingues, P.; Domingues, M. R. M.; Amado, F. M. L.; Ferrer-Correia, A. J. Detection and Characterization of Hydroxyl Radical Adducts by Mass Spectrometry. *J. Am. Soc. Mass Spectrom.* **2001**, *12* (11), 1214−1219.

(24) Guo, Q.; Qian, S. Y.; Mason, R. P. Separation and Identification of DMPO Adducts of Oxygen-Centered Radicals Formed from Organic Hydroperoxides by HPLC-ESR, ESI-MS and MS/MS. *J. Am. Soc. Mass Spectrom.* **2003**, *14* (8), 862−871.

(25) Iwahashi, H.; Parker, C. E.; Mason, R. P.; Tomer, K. B. Combined Liquid Chromatography/Electron Paramagnetic Resonance Spectrometry/Electrospray Ionization Mass Spectrometry for Radical Identification. *Anal. Chem.* **1992**, *64* (19), 2244−2252.
(26) Maurel, V.; Ravanat, J.-L.; Gambarelli, S. Detection of Reactive Free Radicals Derived from Nucleosides by Liquid Chromatography Coupled to Tandem Mass Spectrometry of DMPO Spin Trapping Adducts. *Rapid Commun. Mass Spectrom.* **2006**, *20* (15), 2235−2242.
(27) Reis, A.; Domingues, M. R. M.; Oliveira, M. M.; Domingues, P. Identification of Free Radicals by Spin Trapping with DEPMPO and MCPIO Using Tandem Mass Spectrometry. *Eur. J. Mass Spectrom.* **2009**, *15* (6), 689−703.
(28) Reis, A.; Domingues, P.; Ferrer-Correia, A. J. V.; Domingues, M. R. M. Identification of Free Radicals of Glycerophosphatidylcholines Containing ω-6 Fatty Acids Using Spin Trapping Coupled with Tandem Mass Spectrometry. *Free Radical Res.* **2007**, *41* (4), 432−443.
(29) Yang, F.; Zhang, R.; He, J.; Abliz, Z. Development of a Liquid Chromatography/Electrospray Ionization Tandem Mass Spectrometric Method for the Determination of Hydroxyl Radical. *Rapid Commun. Mass Spectrom.* **2007**, *21* (2), 107−111.
(30) Zoia, L.; Argyropoulos, D. S. Characterization of Free Radical Spin Adducts of 5-Diisopropyloxy-Phosphoryl-5-Methyl-1-Pyrroline-*N* -Oxide Using Mass Spectrometry and ^{31}P Nuclear Magnetic Resonance. *Eur. J. Mass Spectrom.* **2010**, *16* (2), 175−185.
(31) Zhang, X.; Wang, H.; Guo, Y. Interception of the Radicals Produced in Electrophilic Fluorination with Radical Traps (Tempo, Dmpo) Studied by Electrospray Ionization Mass Spectrometry. *Rapid Commun. Mass Spectrom.* **2006**, *20* (12), 1877−1882.
(32) Parker, C. E.; Iwahashi, H.; Tomer, K. B. Spin-Trapped Radicals: Determination by LC-TSP-MS and LC-ESI-MS. *J. Am. Soc. Mass Spectrom.* **1991**, *2* (5), 413−418.
(33) Tong, H.; Lakey, P. S. J.; Arangio, A. M.; Socorro, J.; Shen, F.; Lucas, K.; Brune, W. H.; Pöschl, U.; Shiraiwa, M. Reactive Oxygen Species Formed by Secondary Organic Aerosols in Water and Surrogate Lung Fluid. *Environ. Sci. Technol.* **2018**, 11642−11651.
(34) Mishra, S. S.; Manzoor, K.; Zafar, M.; Podmore, I. D. A Novel Approach to the Analysis of Spin-Trapped Free Radicals Using Dimethyl Sulfoxide and Gas Chromatography − Mass Spectrometry (GC-MS) with Both Solvent Extraction and Headspace Solid Phase Microextraction (HS-SPME). *Free Radical Res.* **2021**, *55* (5), 569−578.
(35) Manzoor, K.; Mishra, S. K.; Podmore, I. D. Detection and Identification of Ethanal-Derived Spin-Trapped Free Radicals Using Headspace Thermal Desorption Gas Chromatography-Mass Spectrometry (TD-GC-MS). *Free Radical Res.* **2020**, *54* (10), 745−755.
(36) Janzen, E. G.; Weber, J. R.; Haire, D. L.; Fung, D. M. Gas Chromatography - Mass Spectroscopy (GC/MS) of Single and Double Spin Adducts of PBN and the Hydroxylamines of Corresponding Structure. *Anal. Lett.* **1985**, *18* (14), 1749−1757.
(37) Janzen, E. G.; Krygsman, P. H.; Lindsay, D. A.; Haire, D. L. Detection of Alkyl, Alkoxyl, and Alkyperoxyl Radicals from the Thermolysis of Azobis(Isobutyronitrile) by ESR/Spin Trapping. Evidence for Double Spin Adducts from Liquid-Phase Chromatography and Mass Spectroscopy. *J. Am. Chem. Soc.* **1990**, *112* (23), 8279−8284.
(38) Yue Qian, S.; Kadiiska, M. B.; Guo, Q.; Mason, R. P. A Novel Protocol to Identify and Quantify All Spin Trapped Free Radicals from in Vitro/in Vivo Interaction of HO and DMSO: LC/ESR, LC/MS, and Dual Spin Trapping Combinations. *Free Radical Biol. Med.* **2005**, *38* (1), 125−135.
(39) Podmore, I.; Cunliffe, L.; Heshmati, M. Rapid Detection of Free Radicals Using Spin Trapping and Maldi-Tof Mass Spectrometry. *J. Chem. Res.* **2013**, *37* (1), 45−47.
(40) Boyd, S. L.; Boyd, R. J. A Theoretical Study of Spin Trapping by Nitrone: Trapping of Hydrogen, Methyl, Hydroxyl, and Peroxyl Radicals. *J. Phys. Chem.* **1994**, *98* (45), 11705−11713.
(41) Jurva, U.; Wikström, H. V.; Bruins, A. P. Electrochemically Assisted Fenton Reaction: Reaction of Hydroxyl Radicals with Xenobiotics Followed by on-Line Analysis with High-Performance Liquid Chromatography/Tandem Mass Spectrometry: Analysis of Fenton Reaction Products by HPLC/MS/MS. *Rapid Commun. Mass Spectrom.* **2002**, *16* (20), 1934−1940.
(42) Medina-Ramos, W.; Mojica, M. A.; Cope, E. D.; Hart, R. J.; Pollet, P.; Eckert, C. A.; Liotta, C. L. Water at Elevated Temperatures (WET): Reactant, Catalyst, and Solvent in the Selective Hydrolysis of Protecting Groups. *Green Chem.* **2014**, *16* (4), 2147−2155.
(43) Steckel, A.; Schlosser, G. An Organic Chemist's Guide to Electrospray Mass Spectrometric Structure Elucidation. *Molecules* **2019**, *24* (3), 611.
(44) Niessen, W. M. A.; Correa, R. A. Fragmentation of Even-Electron Ions. In *Interpretation of MS-MS mass spectra of drugs and pesticides*; Wiley: Hoboken, NJ, 2017, pp. 71−128.
(45) Golubev, V. A.; Sen', V. D.; Kulyk, I. V.; Aleksandrov, A. L. Mechanism of the Oxygen Disproportionation of Ditert-Alkylniteoxyl Radicals. *Russ. Chem. Bull.* **1975**, *24* (10), 2119−2126.
(46) Prescott, C.; Bottle, S. E. Biological Relevance of Free Radicals and Nitroxides. *Cell Biochem. Biophys.* **2017**, *75* (2), 227−240.
(47) Amar, M.; Bar, S.; Iron, M. A.; Toledo, H.; Tumanskii, B.; Shimon, L. J. W.; Botoshansky, M.; Fridman, N.; Szpilman, A. M. Design Concept for α-Hydrogen-Substituted Nitroxides. *Nat. Commun.* **2015**, *6* (1), 6070.
(48) Adamic, K.; Bowman, D. F.; Ingold, K. U. Self-Reaction of Diethylnitroxide Radicals. *J. Am. Chem. Soc.* **1970**, *92* (4), 1093−1094.
(49) Tikhonov, I. V.; Sen', V. D.; Borodin, L. I.; Pliss, E. M.; Golubev, V. A.; Rusakov, A. I. Effect of the Structure of Nitroxyl Radicals on the Kinetics of Their Acid-Catalyzed Disproportionation: Effect of the Structure of Nitroxyl Radicals. *J. Phys. Org. Chem.* **2014**, *27* (2), 114−120.
(50) Pennington, J.; Cohen, R. D.; Tian, Y.; Boulineau, F. Development of an LC−MS Method for Ultra Trace-Level Determination of 2,2,6,6-Tetramethylpiperidine-1-Oxl (TEMPO), a Potential Genotoxic Impurity within Active Pharmaceutical Ingredients. *J. Pharm. Biomed. Anal.* **2015**, *114*, 488−492.
(51) Harada, N. HPLC Separation of Diastereomers: Chiral Molecular Tools Useful for the Preparation of Enantiopure Compounds and Simultaneous Determination of Their Absolute Configurations. *Molecules* **2016**, *21* (10), 1328.
(52) Demarque, D. P.; Crotti, A. E. M.; Vessecchi, R.; Lopes, J. L. C.; Lopes, N. P. Fragmentation Reactions Using Electrospray Ionization Mass Spectrometry: An Important Tool for the Structural Elucidation and Characterization of Synthetic and Natural Products. *Nat. Prod. Rep.* **2016**, *33* (3), 432−455.
(53) Pritsos, C. A.; Constantinides, P. P.; Tritton, T. R.; Heimbrook, D. C.; Sartorelli, A. C. Use of High-Performance Liquid Chromatography to Detect Hydroxyl and Superoxide Radicals Generated from Mitomycin C. *Anal. Biochem.* **1985**, *150* (2), 294−299.
(54) Tian, Y.-W.; Sun, S.-H.; Xie, J.-P.; Zong, Y.-L.; Nie, C.; Guo, Y.-L. Detection of Radical Adducts with Small Molecular Weights by Matrix-Assisted Laser Desorption/Ionization with Fourier Transform Mass Spectrometry. *Chin. J. Chem.* **2007**, *25* (8), 1139−1144.

https://doi.org/10.1021/acs.jpca.4c05311
J. Phys. Chem. A 2024, 128, 10240−10249